

# Direct measurement of hyperfine shifts and radiofrequency manipulation of the nuclear spins in individual CdTe/ZnTe quantum dots

G. Ragunathan,<sup>1,\*</sup> J. Kobak,<sup>1,2,†</sup> G. Gillard,<sup>1</sup> W. Pacuski,<sup>2</sup> K. Sobczak,<sup>3</sup> J. Borysiuk,<sup>2</sup> M. S. Skolnick,<sup>1</sup> and E. A. Chekhovich<sup>1,‡</sup>

<sup>1</sup>*Department of Physics and Astronomy, University of Sheffield, Sheffield, S3 7RH, UK*

<sup>2</sup>*Institute of Experimental Physics, Faculty of Physics,*

*University of Warsaw, ul. Pasteura 5, 02-093 Warsaw, Poland*

<sup>3</sup>*Biological and Chemical Research Centre, Faculty of Chemistry,*

*University of Warsaw, ul. Żwirki i Wigury 101, 02-089 Warsaw, Poland*

(Dated: July 20, 2018)

We achieve direct detection of electron hyperfine shifts in individual CdTe/ZnTe quantum dots. For the previously inaccessible regime of strong magnetic fields  $B_z \gtrsim 0.1$  T, we demonstrate robust polarization of a few-hundred-particle nuclear spin bath, with optical initialization time of  $\sim 1$  ms and polarization lifetime exceeding  $\sim 1$  s. Nuclear magnetic resonance spectroscopy of individual dots reveals strong electron-nuclear interactions characterized by the Knight fields  $|B_e| \gtrsim 50$  mT, an order of magnitude stronger than in III-V semiconductor quantum dots. Our studies confirm II-VI semiconductor quantum dots as a promising platform for hybrid electron-nuclear spin quantum registers, combining the excellent optical properties comparable to III-V dots, and the dilute nuclear spin environment similar to group-IV semiconductors.

The proposed designs for solid-state quantum information processing devices require two essential components: the quantum nodes for storing and processing information, and the quantum channels connecting the nodes<sup>1</sup>. Various material systems using single spins as qubit nodes and single photons as channels have been considered. III-V semiconductor quantum dots (QDs) are of particular interest, since they benefit from mature epitaxial technologies and exceptional single-photon properties<sup>2-4</sup>. However, the electron spin qubits<sup>5</sup> suffer fast decoherence due to the interaction with a dense nuclear spin environment<sup>6,7</sup>. By contrast, group IV semiconductors, such as silicon and diamond, where most nuclei are spin-free ( $I = 0$ ) offer defect-spin qubits with record coherence<sup>8,9</sup>, while their optical properties and fabrication technology are inherently limited. The advantages of the two approaches can be combined if optically active quantum dots can be grown of materials with spin-free nuclei. The II-VI semiconductors are a natural choice for this since most nuclei are spin-free and the direct-bandgap character offers a good interface between electron spin and photons.

The research of the past two decades have lead to an in-depth understanding and development of advanced techniques for probing and manipulation of the nanoscale nuclear spin ensembles in III-V QDs<sup>6,7</sup>. By contrast, current understanding of the nuclear spin phenomena in II-VI dots is scarce, due to the challenges arising from the small nuclear spin magnetisation in a dilute spin bath. Previous studies<sup>10-13</sup> relied on indirect detection of the nuclear spin effects via probing of the electron spin dynamics. Consequently, these experiments were restricted to low magnetic fields ( $B \lesssim 0.1$  T), leaving beyond reach the most interesting regime where nonsecular electron-nuclear spin interactions are suppressed by magnetic field giving access to long-lived electron and nuclear spin states, required for qubit applications.

Here we achieve direct probing of the nuclear spin state by measuring Overhauser spectral shifts in individual CdTe/ZnTe quantum dots, which enables studies in a wide range of external fields. A cascade relaxation process involving quantum well states is identified as a source of efficient dynamic nuclear polarization (DNP) in magnetic fields up to 8 T. The DNP can be induced within  $\sim 1$  ms and persists in the dark over  $\sim 1$  s, three orders of magnitude longer than observed previously in II-VI QDs at low fields. The direct detection of spectral shifts employed here, reveals an additional effect which mimics DNP, but is characterized by submicrosecond timescales pointing to electron spin interactions as a source. While in previous studies nuclear species could not be addressed individually, here we measure cadmium and tellurium nuclear magnetic resonance signals in individual CdTe dots and observe strong electron-nuclear interaction characterized by the Knight fields exceeding 50 mT. Our results suggest CdTe/ZnTe quantum dots as a promising system with a potential of implementing a hybrid quantum spin register architecture<sup>14</sup> based on one electron coupled to few individually addressable nuclei, and with high optical efficiency unachievable in group-IV semiconductors.

We study two CdTe/ZnTe samples grown by molecular beam epitaxy. In sample A, low-density QDs were formed using the amorphous Te technique<sup>15,16</sup>, whereas in sample B, amorphous Te deposition was avoided, resulting in a higher QD density and preservation of the CdTe wetting layer quantum well (for further details see Supplemental Material Note 1). Micro-photoluminescence ( $\mu$ -PL) experiments are conducted at a temperature of 4.2 K with an external magnetic field  $B_z$  applied along the sample growth axis (Faraday geometry). PL of individual QDs is excited non resonantly using a solid-state laser emitting at 532 nm or 561 nm, and the emission of a neutral exciton ( $X^0$ ) state is collected and dispersed by a 1 m double spectrometer, followed by a pair of achro-

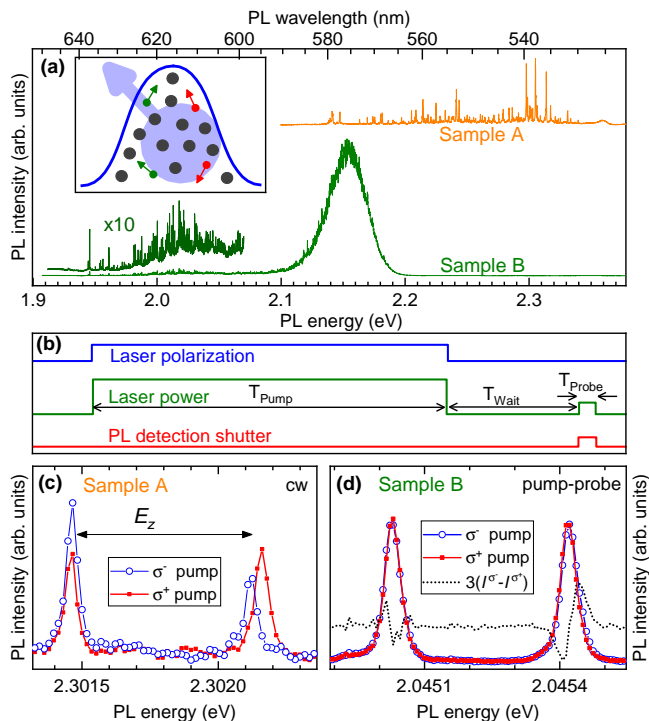


FIG. 1. (a) Broad range photoluminescence (PL) spectra from CdTe/ZnTe samples A (top) and B (bottom) under 405 nm laser excitation. PL spectrum of sample A consists of QD emission at 2.13 – 2.34 eV and a weak ZnTe barrier peak at 2.36 eV. Sample B spectrum includes QDs at 1.94 – 2.09 eV and CdTe quantum well emission centered at 2.155 eV. Inset shows schematic of the quantum dot electron spin (large arrowhead) interacting with only a few spin-1/2 nuclei (small arrowheads) randomly distributed among spin-0 nuclei (small circles). (b) Timing of the pump-probe measurement cycle, where laser polarization, power, and PL detection are controlled separately to implement pump and probe pulses with different characteristics. (c) Continuous wave (cw) PL spectra of a single CdTe/ZnTe neutral QD from sample A under  $\sigma^-$  (circles) and  $\sigma^+$  (squares) excitation at  $B_z = 4$  T. A visible change in splitting  $E_Z^{\sigma^-} - E_Z^{\sigma^+} \approx -44 \mu\text{eV}$  is detected but is not related to nuclear spin effects. (d) Pump-probe PL spectra of a single CdTe/ZnTe neutral QD from sample B measured at  $B_z = 2.5$  T with linearly polarized probe and  $\sigma^-$  (circles) or  $\sigma^+$  (squares) pump using  $T_{\text{Pump}} = 40$  ms,  $T_{\text{Wait}} = 4.5$  ms,  $T_{\text{Probe}} = 1$  ms. The change in Zeeman splitting  $E_Z^{\sigma^-} - E_Z^{\sigma^+} \approx 4 \mu\text{eV}$  is smaller than the linewidth (36  $\mu\text{eV}$ ), but is revealed in the difference spectrum (dotted line,  $\times 3$  scaled for clarity) and is ascribed to dynamic nuclear polarization.

matic doublets, which transfers the spectral image onto the charge coupled device (CCD) detector with a linear magnification of 3.75. Using Gaussian fitting it is possible to detect the change in splitting of spectral peaks with an accuracy of  $\sim 0.5 \mu\text{eV}$ . In order to implement pump-probe measurements, the polarization of the laser is modulated with an electro-optical modulator (Pockels cell, response time  $\approx 0.5 \mu\text{s}$ ), while analogue modulation of the

diode pump current is used to modulate the power of the laser (response time  $< 1 \mu\text{s}$ ) from the nominal power to zero. The PL signal is modulated with an acousto-optic modulator (response time  $\approx 1.1 \mu\text{s}$ , on/off ratio  $> 1000$ ) or a liquid crystal cell (response time  $\approx 4.5$  ms, on/off ratio  $> 5000$ ).

Fig. 1(a) shows broad-range PL spectra of samples A and B. Both structures exhibit sharp spectral lines characteristic of QD emission with full width at half maximum as low as  $\sim 30 \mu\text{eV}$  in sample A and  $\sim 20 \mu\text{eV}$  in sample B. For sample B, a strong, broad PL peak arising from QW emission is observed at  $\sim 2.15$  eV, and the number of sharp peaks is an order of magnitude higher than in sample A, confirming the higher dot density in sample B. In most studied individual QDs, PL is dominated by recombination of a bright neutral exciton, recognized through its fine structure splitting. In an external magnetic field  $B_z$ , the bright exciton localized in a QD becomes a doublet of states with electron spin parallel or antiparallel to  $B_z$  and with Zeeman energy splitting  $E_Z$ . Nuclear spins polarized along the  $z$  axis act on the electron via the hyperfine interaction and shift the exciton energies in opposite directions, which can be observed in the PL spectrum as a change in  $E_Z$ <sup>6,7</sup>. In III-V QDs excitation with  $\sigma^+$  or  $\sigma^-$  circularly polarized light results in repeated injection of spin polarized electrons into the dot, leading to DNP of the dot nuclei via hyperfine interaction. The resulting variation in the exciton Zeeman splitting can be as large as  $|E_Z^{\sigma^+} - E_Z^{\sigma^-}| > 200 \mu\text{eV}$ , significantly exceeding the PL linewidths, and a pronounced effect is observed<sup>6,7,17</sup>.

Using the same approach, we measure PL spectra under  $\sigma^+$  or  $\sigma^-$  excitation at 532 nm in CdTe/ZnTe QDs. A typical result for a single QD in sample A is presented in Fig. 1(c) where a noticeable ( $\sim 44 \mu\text{eV}$ ) change in  $E_Z$  is detected. Although this result is reminiscent of how DNP manifests in III-V dots, in some CdTe/ZnTe dots variation of  $E_Z$  exceeds that expected for  $\pm 100\%$  nuclear spin polarization. To verify this effect, additional pump-probe measurements were conducted with pulse timing shown in Fig. 1(b). In this experiment, the dot is periodically excited with a pump pulse with a variable degree of circular polarization (e.g.  $\sigma^+$ ,  $\sigma^-$  or linear), while the PL is detected only during a subsequent short probe pulse with a fixed linear polarization. The key feature of this experiment is that the observed splitting  $E_Z$  is sensitive only to those effects of the pump that persist over a sufficiently long time  $T_{\text{Wait}}$ , as should be the case for nuclear spin polarization whose lifetime is orders of magnitude longer than the exciton radiative recombination time of a few hundred picoseconds.

While nearly 15% out of  $\sim 90$  individual QDs examined in sample A showed a pronounced change in  $E_Z$  in continuous wave (cw) PL [see Fig. 1(c)], surprisingly, no measurable change in  $E_Z$  could be detected in pump-probe experiments with either 532 nm or 561 nm excitation. Moreover, additional dynamics measurements have shown that the change in  $E_Z$  induced by a circularly po-

larized pump persists for less than  $T_{\text{Wait}} < 0.5 \mu\text{s}$  (limited by modulators resolution), which is too short to be ascribed to nuclear spin polarization dynamics. The exact origin of the changes in  $E_Z$  in cw PL is not yet clear and requires further investigation. The effect is absent for 561 nm excitation but is observed under 532 nm excitation, and only for the dots with small detuning from the laser (QD ground state emission between 537 nm and 539 nm). Based on the sub-microsecond timescales it is likely to be related to electron or hole spin effects, for example dipolar and/or exchange interaction with spin polarized charges in nearby quantum dots or defects.

Having established the absence of DNP in sample A, we have conducted pump-probe experiments on QDs in sample B using 561 nm pump laser, with a typical result presented in Fig. 1(d). The change in Zeeman splitting  $E_Z^{\sigma^-} - E_Z^{\sigma^+} \approx 4 \mu\text{eV}$  is smaller than the PL linewidths, but is detected reliably from Gaussian lineshape fitting. Similar results were obtained from the measurements on  $\sim 20$  individual QDs from sample B. The systematic nature and the sign (see Supplemental Note 3) of the shift observed in pump-probe measurements suggests DNP as its origin. Further investigation is presented in Fig. 2(a) where power dependent measurements are shown: at low power,  $E_Z$  (squares) does not depend on polarization of the pump, but at higher power, a clear increase (decrease) in  $E_Z$  is observed under  $\sigma^-$  ( $\sigma^+$ ) pumping, saturating above  $\sim 50 \mu\text{W}$ , which corresponds to the saturation power of the bright neutral exciton PL intensity (triangles). Such saturation is observed in all studied dots in sample B, which is different from the III-V QDs (InGaAs/GaAs, GaAs/AlGaAs, InP/GaInP) where DNP under non-resonant optical excitation is often found to be most efficient at optical powers significantly exceeding the saturation of the ground state<sup>18–20</sup>, implying the role of multi-exciton and excited QD states.

Fig. 2(b) shows the dependence of the DNP measured as the difference  $E_Z^{\sigma^-} - E_Z^{\sigma^+}$  in a QD in sample B at different magnetic fields  $B_z$ . DNP is nearly absent at zero field but becomes more efficient with applied field, reaching a maximum at  $B_z \approx 2.5 \text{ T}$ . Such an increase with  $B_z$  can be explained as follows: At  $B_z = 0 \text{ T}$ , bright exciton states have no electron spin polarization due to the fine structure splitting ( $\delta_b \approx 115 \mu\text{eV}$  for this dot) and thus can not interact with nuclear spins. With applied magnetic field, exciton Zeeman splitting increases ( $\approx 150 \mu\text{eV/T}$  for this dot, see Supplemental Note 2) restoring electron spin polarization of the exciton states and re-enabling interaction with the nuclei. At large magnetic fields significant DNP is observed up to  $B_z = 8 \text{ T}$ , the partial reduction of DNP above 2.5 T is similar to that observed in III-V QDs<sup>21</sup> and is likely due to the mismatch in the electron and nuclear spin energy splitting, which increases with magnetic field, slowing down DNP.

Experimental observations presented above allow to make general conclusions about the mechanism of DNP. Saturation of the nuclear spin polarization level with sat-

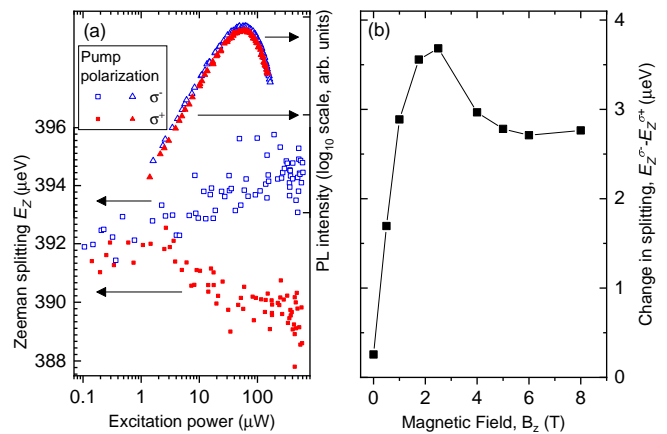


FIG. 2. (a) Total PL intensity (sum for two Zeeman components) of a QD from sample B measured in cw (triangles, right scale), and Zeeman splitting  $E_Z$  measured in pump-probe (squares) as a function of power under  $\sigma^-$  (open symbols) and  $\sigma^+$  (solid symbols) 561 nm laser excitation at  $B_z = 2.5 \text{ T}$ . (b) Magnetic field dependence of the change in Zeeman splitting  $E_Z^{\sigma^-} - E_Z^{\sigma^+}$  measured on the same quantum dot in pump-probe experiment with pump duration  $T_{\text{Pump}} = 40 \text{ ms}$  and power  $160 \mu\text{W}$ .

uration of the QD ground state PL, as well suppression of DNP at low magnetic fields where fine structure splitting dominates point to the key role of the neutral exciton spin states. On the other hand, DNP is found to be efficient only in structure B, where quantum well states are present in addition to QD states. This is despite the fact that circularly polarized optical excitation produces similar exciton spin polarization degrees in both structures: exciton spin polarization is evidenced in Fig. 1(c) where  $\sigma^+$  ( $\sigma^-$ ) excitation enhances PL intensity  $I_h$  ( $I_l$ ) of the high (low) energy exciton state, and the difference in PL polarization degrees  $\rho = (I_h - I_l)/(I_h + I_l)$  under  $\sigma^+$  and  $\sigma^-$  excitation is  $\Delta\rho \approx (+0.11) - (-0.35) = 0.45$ . We find similar  $\Delta\rho$  values for QDs in both samples while DNP is observed only in sample B, suggesting that DNP takes place not during ground state radiative lifetime or recombination, but rather during the initial relaxation and formation of the QD ground state exciton. This interpretation is supported by the presence of the intermediate quantum well states in sample B, which appear to be a critical factor for efficient spin exchange between the electrons and nuclei.

Focusing on sample B we now turn to investigation of the nuclear spin dynamics in individual CdTe/ZnTe QDs. Open (solid) symbols in Fig. 3(a) show the buildup dynamics of the DNP under  $\sigma^-$  ( $\sigma^+$ ) pumping measured at  $B_z = 2.5 \text{ T}$ , where exponential fitting (lines) reveals characteristic build up time of  $\tau_{\text{Buildup}} \sim 1 \text{ ms}$ . Similar  $\tau_{\text{Buildup}}$  were observed on different individual QDs at  $B_z = 2.5 \text{ T}$ . These  $\tau_{\text{Buildup}}$  values are a factor of  $\sim 1000$  smaller than  $\tau_{\text{Buildup}} \sim 0.5 - 3 \text{ s}$  found in III-V QDs at high magnetic fields<sup>20–23</sup>. One of the contributions to shorter  $\tau_{\text{Buildup}}$  is the smaller abundance of magnetic

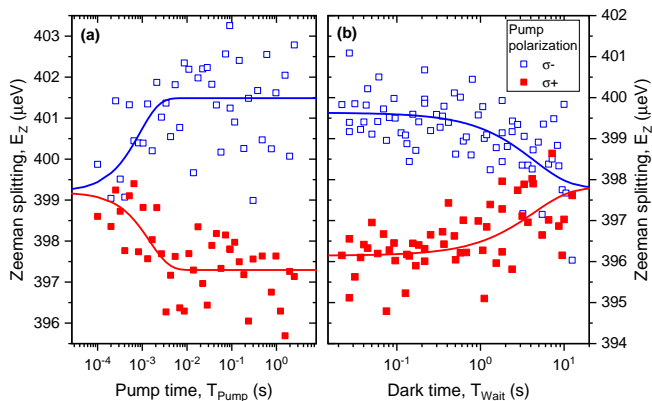


FIG. 3. (a) Buildup dynamics of the optically induced nuclear spin polarization in a single QD at  $B_z = 2.5$  T, measured with a pump-probe cycle shown in Fig. 1(b), but with the addition of an erase laser pulse (duration  $T_{\text{Erase}} = 50$  ms, power  $160 \mu\text{W}$ , linearly polarized) preceding each pump pulse. Probe pulse power and duration are  $20 \mu\text{W}$  and  $T_{\text{Probe}} = 1$  ms. Open (solid) symbols show experiment with  $\sigma^-$  ( $\sigma^+$ ) polarized pump, lines show exponential fitting yielding 95% confidence intervals for the buildup time:  $\tau_{\text{Buildup}} = 0.9^{+1.3}_{-0.5}$  ms ( $1.5^{+3.0}_{-1.0}$  ms). (b) Decay of the nuclear spin polarization measured using the cycle of Fig. 1(b) with variable dark time  $T_{\text{Wait}}$  and fixed  $T_{\text{Pump}} = 40$  ms,  $T_{\text{Probe}} = 1$  ms. The nuclear spin lifetime derived from the exponential fit (lines) is  $\tau_{\text{Decay}} = 4.3^{+2.5}_{-1.6}$  s (95% confidence).

isotopes ( $\sim 25\%$  for Cd and  $\sim 8\%$  for Te, compared to 100% for group III and V nuclei) and smaller spin number  $I = 1/2$  (as opposed to  $I = 3/2$  for Ga and As, and  $I = 9/2$  for In), which requires fewer electron-nuclear flip-flops to approach equilibrium nuclear spin polarization in CdTe QDs. However, based on lower  $I$  and abundance alone, one would expect a factor of  $\sim 30$  shorter  $\tau_{\text{Buildup}}$  for CdTe. The remaining difference is due to a smaller QD volume, typically containing  $\sim 5 \times 10^3$  atoms (based on transmission electron microscopy, see Supplementary Note 1), as opposed to  $10^4$ - $10^5$  atoms in III-V QDs. The buildup time  $\tau_{\text{Buildup}} \sim 1$  ms observed here at  $B_z = 2.5$  T is an order of magnitude longer than the  $< 100 \mu\text{s}$  time found previously in CdTe/ZnTe<sup>13</sup> and CdSe/ZnSe<sup>10</sup> dots at low magnetic fields, which is well explained by the reduction of the electron-nuclear spin flip-flop probability due to the increasing mismatch in the Zeeman energies.

The measurement of the nuclear spin polarization decay in the dark, following excitation with a  $\sigma^-$  ( $\sigma^+$ ) polarized pump is shown in Fig. 3(b) by the open (solid) symbols. At long waiting times nuclear polarization is seen to decay almost completely, with characteristic time  $\tau_{\text{Decay}} \sim 4$  s deduced from exponential fitting (lines). Similar  $\tau_{\text{Decay}}$  were observed in several individual CdTe quantum dots in sample B and are significantly longer than submillisecond  $\tau_{\text{Decay}}$  reported for charged CdSe QDs at low magnetic fields<sup>11</sup>, but are noticeably shorter than  $\tau_{\text{Decay}} \sim 10^2 - 10^5$  s observed both in neutral<sup>21,22</sup> and charged<sup>24,25</sup> III-V quantum dots at

high magnetic field. The long  $\tau_{\text{Decay}}$  in III-V QDs are due to the strain-induced quadrupolar effects which inhibit spin diffusion via nuclear dipolar flip-flops. Although quadrupolar effects are absent for the spin  $I = 1/2$  nuclei in CdTe/ZnTe dots, the observed  $\tau_{\text{Decay}}$  is too short to be ascribed to spin diffusion alone. The most likely cause of fast DNP decay is the electron-nuclear interaction<sup>24,25</sup>. Although the PL of the studied QDs is dominated by the neutral exciton state, the effect of the fluctuating charge environment (nearby QDs and/or charge traps) is evidenced in spectral wandering of the PL energy (the wandering differs from dot to dot and is within  $\sim 100 \mu\text{eV}$  over the time scales of hours for the best QDs, see details in Supplementary Note 4). Moreover, it is possible that the studied dot itself is intermittently occupied by electrons or holes leading to nuclear spin depolarization<sup>21</sup>. As we show below, NMR spectroscopy corroborates this interpretation.

While optical methods can be used to manipulate and detect QD nuclear spin magnetization along the external field, a complete control of the magnetization vector requires radio frequency (RF) magnetic fields. Figure 4 shows nuclear magnetic resonance (NMR) spectra, obtained by depolarizing the nuclei with RF field of a variable frequency  $f_{\text{RF}}$ . In order to balance NMR spectral resolution and signal amplitude, the RF signal contains multiple frequencies and has a shape of a rectangular spectral band centered at  $f_{\text{RF}}$  (see details in Supplementary Note 5). Measurement on QD1 conducted at  $B_z \approx 2.5$  T with a  $\sigma^-$  pump and a resolution of 174 kHz are presented in Fig. 4(a) and show resolution limited negative peaks at  $\sim 22.6$  MHz and  $\sim 33.7$  MHz, which indicate nuclear spin depolarization at the expected resonance frequencies of <sup>111</sup>Cd and <sup>125</sup>Te. From the NMR peak amplitude, the total Cd hyperfine shift is  $\sim 0.8 \mu\text{eV}$ . Using the known electron wavefunction density in CdTe<sup>26</sup>, we find Cd polarization degree  $\gtrsim 15\%$ , which is a lower bound since the electron wavefunction is partly localized in the ZnTe barrier. (NMR has not been detected on <sup>67</sup>Zn, due to its low abundance and quadrupolar broadening).

Similar NMR measurements on another individual dot [QD2, Fig. 4(b)] show a more complex picture. A clear peak-like structure is observed only for the measurement on Cd nuclei ( $\sim 22.2 - 23.3$  MHz) with  $\sigma^-$  pumping. Measurement with a 174 kHz resolution (solid line) shows a combination of a resolution limited negative peak ( $\sim -0.5 \mu\text{eV}$  amplitude) and a flat background offset of  $\sim -0.3 \mu\text{eV}$  with respect to the Zeeman splitting measured without RF (horizontal dashed line). As NMR measurements reveal complex spectra, we have conducted additional measurements in the  $\sim 25.4 - 26.2$  MHz frequency range [see Fig. 4(b)] corresponding to RF detuned from all isotopes. The data reveals only fluctuations with a  $\sim 0.5 \mu\text{eV}$  peak-to-peak amplitude, without any systematic offset from the reference level measured without RF (dashed lines). This confirms that the broad ( $> 1$  MHz width) background offsets observed

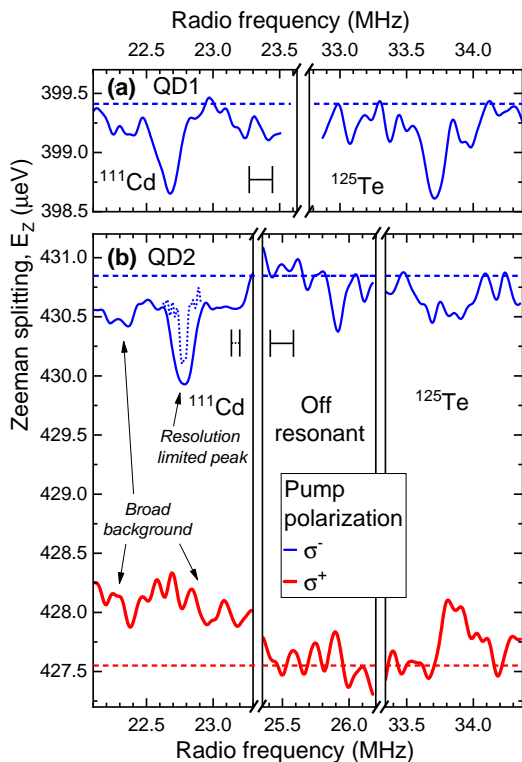


FIG. 4. Optically detected NMR spectra in CdTe/ZnTe quantum dots of sample B at  $B_z \approx 2.5$  T. Timing diagram of Fig. 1(b) is used in this measurement with RF pulse applied during the  $T_{\text{Wait}}$ . The RF excitation pulse has a rectangular-band spectrum with a width of 63 kHz (dotted lines) and 174 kHz (solid lines) which determines spectral resolution (also shown by the horizontal bars). The RF pulse duration is  $T_{\text{RF}} = 50 - 120$  ms. In order to increase the signal, all cadmium NMR spectra are recorded by combining the signals from  $^{111}\text{Cd}$  and  $^{113}\text{Cd}$ . This is achieved using two RF spectral bands, where the mean frequency of the second band  $f_{113\text{Cd}} = (\gamma_{113\text{Cd}}/\gamma_{111\text{Cd}})f_{111\text{Cd}}$  is the frequency of the main band  $f_{111\text{Cd}}$  scaled by the ratio of the gyromagnetic values  $\gamma_{113\text{Cd}}/\gamma_{111\text{Cd}} = 9.487/9.069$ . (a) Zeeman splitting  $E_z$  in QD1 as a function of radio frequency measured with a  $\sigma^-$  pump. Dashed horizontal line shows  $E_z$  measured without RF. Negative peaks are observed at  $\sim 22.6$  MHz and  $\sim 33.7$  MHz corresponding to RF depolarization of  $^{111}\text{Cd}$  and  $^{125}\text{Te}$  nuclei respectively. (b) NMR measurements on QD2 with  $\sigma^-$  (thin blue lines) and  $\sigma^+$  (thick red lines) pump. The observed NMR spectra are a combination of resolution limited peaks and broad background. Measurements at  $\sim 25.5 - 26.0$  MHz are out of resonance with all isotopes and demonstrate typical noise levels.

in Cd measurements as well as broad (width  $> 300$  kHz) peaks in Te measurements on QD2 are real NMR signals and are not related for example to RF-induced sample heating.

The spin-1/2 nuclei are insensitive to electric field gradients, while the nuclear-nuclear dipolar interactions are limited to few kHz. This leaves the effective field  $B_e$  of the electron spin (Knight field) as the only source of the

broad background in the NMR spectra. The Knight shift of  $^{111}\text{Cd}$  equals  $\gamma_{111\text{Cd}}B_e$  and is at least  $\sim \pm 0.5$  MHz in QD2, leading to the estimate  $|B_e| \gtrsim 50$  mT. Such a large  $B_e$  can be generated by electrons intermittently occupying the dot during RF excitation in the dark. The time-averaged NMR spectrum of  $^{111}\text{Cd}$  under  $\sigma^-$  pump [see Fig. 4(b)] is then explained as a sum of the narrow peak arising from an empty dot, and a broad offset arising from the electron-charged state of the dot. Note, that in addition to the peaks, the broad background is also observed for QD1 in Fig. 4(a), though to a smaller extent, implying a smaller fraction of time in an electron-charged state. We further note that  $B_e$  estimated here for CdTe QDs is at least a factor of  $\sim 5$  larger than  $|B_e| \sim 10$  mT observed in InGaAs<sup>27</sup> and InP QDs<sup>21</sup>, which agrees with a smaller number of nuclei (with and without spin) within the volume of the electron in a CdTe QD.

Having established the origin of the broad background we examine the resolution limited NMR peak. A further measurement of  $^{111}\text{Cd}$  NMR with a  $\sigma^-$  pump and resolution of 63 kHz [dotted line in Fig. 4(b)] also yields a broad background offset and a resolution limited peak. However the peak amplitude is reduced compared to the 174 kHz measurement. Measurements with even better resolution resulted in amplitude too small to detect, suggesting that the resolution limited peak itself consists of a narrow peak (width  $\lesssim 63$  kHz) and broad ( $\sim 100$  kHz) wings. The width of the wings suggests Knight field as the cause, but unlike the broad background, this smaller broadening of the resolution limited peak is likely to arise from the Knight field of the electrons occupying nearby charge traps and/or QDs which are also responsible for spectral wandering.

In conclusion, we have demonstrated manipulation and probing of the nuclear spins in individual CdTe quantum dots using optical and radiofrequency fields. The direct detection of the electron hyperfine shifts in a pump-probe manner is shown to have a key role in distinguishing between the real nuclear spin phenomena and the effects that mimic DNP. Moreover, the direct detection have enabled exploring arbitrary magnetic fields: at  $B_z \gtrsim 1$  T we achieve fast ( $\sim 1$  ms) initialization and long ( $\gtrsim 1$  s) persistence of the nuclear spin polarization. Unlike III-V semiconductor quantum dots where the nuclear spin bath has a mesoscopic character, II-VI dots offer an attractive alternative with an inherently smaller number of nuclei interacting with the electron and a further potential for a few-spin or spin-free bath via isotope purification. Our results set the direction for further work required to realize this potential: Experiments with quasi-resonant and resonant QD optical excitation can be used to better understand the DNP mechanisms and achieve highly polarized nuclear spin state. Control of the charge state of the quantum dot and its environment (e.g. using gated structures) can overcome inhomogeneous NMR broadening, which in turn will enable coherent manipulation of the nuclear spins. Strong electron-nuclear interaction (observed as large Knight shifts) and the ability to dilute

the nuclear spin bath offer in principle the possibility to address individual nuclear spins with resonant radiofrequency fields. In this way the II-VI quantum dots have potential for implementing the hybrid electron-nuclear spin quantum registers which have been demonstrated in group IV semiconductors<sup>14</sup>, but are not feasible in III-V dots.

## ACKNOWLEDGMENTS

This work was supported by the EPSRC Programme Grant EP/N031776/1. E.A.C. was supported by a University Research Fellowship from the Royal Society. J.K., W.P., and K.S. were supported by the Polish National Science Center (grants DEC-2015/16/T/ST3/00371 and DEC-2015/18/E/ST3/00559).

- 
- \* [gragunathan1@sheffield.ac.uk](mailto:gragunathan1@sheffield.ac.uk)  
† [Jakub.Kobak@fuw.edu.pl](mailto:Jakub.Kobak@fuw.edu.pl)  
‡ [e.chekhovich@sheffield.ac.uk](mailto:e.chekhovich@sheffield.ac.uk)
- <sup>1</sup> H. J. Kimble, *Nature* **453**, 1023 (2008).
  - <sup>2</sup> N. Somaschi, V. Giesz, L. De Santis, J. C. Loredo, M. P. Almeida, G. Hornecker, S. L. Portalupi, T. Grange, C. Anton, J. Demory, C. Gomez, I. Sagnes, N. D. Lanzillotti-Kimura, A. Lemaitre, A. Auffeves, A. G. White, L. L., and S. P., *Nature Photon* **10**, 340 (2016).
  - <sup>3</sup> X. Ding, Y. He, Z.-C. Duan, N. Gregersen, M.-C. Chen, S. Unsleber, S. Maier, C. Schneider, M. Kamp, S. Höfling, C.-Y. Lu, and J.-W. Pan, *Phys. Rev. Lett.* **116**, 020401 (2016).
  - <sup>4</sup> R. Stockill, M. J. Stanley, L. Huthmacher, E. Clarke, M. Hugues, A. J. Miller, C. Matthiesen, C. Le Gall, and M. Atatüre, *Phys. Rev. Lett.* **119**, 010503 (2017).
  - <sup>5</sup> D. Loss and D. P. DiVincenzo, *Phys. Rev. A* **57**, 120 (1998).
  - <sup>6</sup> B. Urbaszek, X. Marie, T. Amand, O. Krebs, P. Voisin, P. Maletinsky, A. Högele, and A. Imamoglu, *Rev. Mod. Phys.* **85**, 79 (2013).
  - <sup>7</sup> E. A. Chekhovich, M. N. Makhonin, A. I. Tartakovskii, A. Yacoby, H. Bluhm, K. C. Nowack, and L. M. K. Vandersypen, *Nature Materials* **12**, 494 (2013).
  - <sup>8</sup> L. Childress, M. V. Gurudev Dutt, J. M. Taylor, A. S. Zibrov, F. Jelezko, J. Wrachtrup, P. R. Hemmer, and M. D. Lukin, *Science* **314**, 281 (2006).
  - <sup>9</sup> J. J. Pla, K. Y. Tan, J. P. Dehollain, W. H. Lim, J. J. L. Morton, D. N. Jamieson, A. S. Dzurak, and A. Morello, *Nature* **489**, 541 (2012).
  - <sup>10</sup> I. A. Akimov, D. H. Feng, and F. Henneberger, *Phys. Rev. Lett.* **97**, 056602 (2006).
  - <sup>11</sup> D. H. Feng, I. A. Akimov, and F. Henneberger, *Phys. Rev. Lett.* **99**, 036604 (2007).
  - <sup>12</sup> J. Kim, J. Puls, Y. S. Chen, G. Bacher, and F. Henneberger, *Appl. Phys. Lett.* **96**, 151908 (2010).
  - <sup>13</sup> C. Le Gall, A. Brunetti, H. Boukari, and L. Besombes, *Phys. Rev. B* **85**, 195312 (2012).
  - <sup>14</sup> M. V. G. Dutt, L. Childress, L. Jiang, E. Togan, J. Maze, F. Jelezko, A. S. Zibrov, P. R. Hemmer, and M. D. Lukin, *Science* **316**, 1312 (2007).
  - <sup>15</sup> F. Tinjod, B. Gilles, S. Moehl, K. Kheng, and H. Mariette, *Appl. Phys. Lett.* **82**, 4340 (2003).
  - <sup>16</sup> J. Kobak, J.-G. Rousset, R. Rudniewski, E. Janik, T. Slupinski, P. Kossacki, A. Golnik, and W. Pacuski, *J. Cryst. Growth* **378**, 274 (2013).
  - <sup>17</sup> D. Gammon, A. L. Efros, T. A. Kennedy, M. Rosen, D. S. Katzer, D. Park, S. W. Brown, V. L. Korenev, and I. A. Merkulov, *Phys. Rev. Lett.* **86**, 5176 (2001).
  - <sup>18</sup> E. A. Chekhovich, A. B. Krysa, M. S. Skolnick, and A. I. Tartakovskii, *Phys. Rev. B* **83**, 125318 (2011).
  - <sup>19</sup> J. Puebla, E. A. Chekhovich, M. Hopkinson, P. Senellart, A. Lemaitre, M. S. Skolnick, and A. I. Tartakovskii, *Phys. Rev. B* **88**, 045306 (2013).
  - <sup>20</sup> A. Ulhaq, Q. Duan, E. Zallo, F. Ding, O. G. Schmidt, A. I. Tartakovskii, M. S. Skolnick, and E. A. Chekhovich, *Phys. Rev. B* **93**, 165306 (2016).
  - <sup>21</sup> E. A. Chekhovich, M. N. Makhonin, J. Skiba-Szymanska, A. B. Krysa, V. D. Kulakovskii, M. S. Skolnick, and A. I. Tartakovskii, *Phys. Rev. B* **81**, 245308 (2010).
  - <sup>22</sup> A. E. Nikolaenko, E. A. Chekhovich, M. N. Makhonin, I. W. Drouzas, A. B. Van'kov, J. Skiba-Szymanska, M. S. Skolnick, P. Senellart, D. Martrou, A. Lemaitre, and A. I. Tartakovskii, *Phys. Rev. B* **79**, 081303 (2009).
  - <sup>23</sup> T. Belhadj, T. Kuroda, C.-M. Simon, T. Amand, T. Mano, K. Sakoda, N. Koguchi, X. Marie, and B. Urbaszek, *Phys. Rev. B* **78**, 205325 (2008).
  - <sup>24</sup> P. Maletinsky, A. Badolato, and A. Imamoglu, *Phys. Rev. Lett.* **99**, 056804 (2007).
  - <sup>25</sup> C. Latta, A. Srivastava, and A. Imamoglu, *Phys. Rev. Lett.* **107**, 167401 (2011).
  - <sup>26</sup> A. Nakamura, D. Paget, C. Hermann, C. Weisbuch, G. Lampel, and B. Cavenett, *Solid State Commun.* **30**, 411 (1979).
  - <sup>27</sup> C. W. Lai, P. Maletinsky, A. Badolato, and A. Imamoglu, *Phys. Rev. Lett.* **96**, 167403 (2006).

## SUPPLEMENTAL MATERIAL

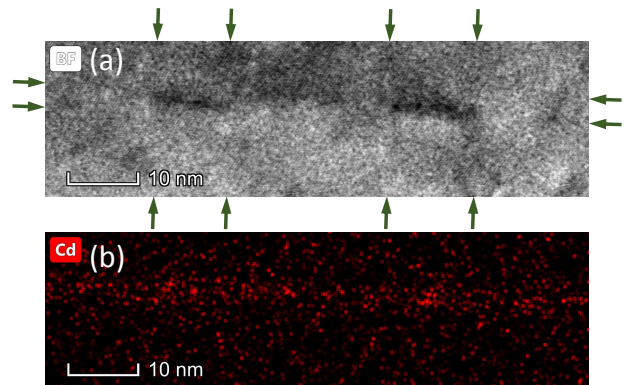
The supplemental material contains additional experimental results supporting the discussion of the main text.

### Supplemental Note 1. CdTe/ZnTe SAMPLE STRUCTURES AND TRANSMISSION ELECTRON MICROSCOPY

We study two CdTe/ZnTe samples grown by molecular beam epitaxy. The samples were grown on GaAs:Si or GaAs:Zn (100) substrates. The growth of a ZnTe buffer layer (1  $\mu\text{m}$  or 1.3  $\mu\text{m}$  thick), was followed by atomic layer epitaxy growth of the CdTe layer. Due to the small energy of dislocation formation in CdTe/ZnTe<sup>S1</sup>, special measures were taken to achieve dislocation-free QD formation. Two approaches were used. In sample A, amorphous Te technique was employed<sup>S1</sup>, where the substrate was strongly cooled (to  $\sim 100$  °C) whilst Te was deposited onto the dot layer. This led to a decrease of the surface energy and the thin CdTe film layer subsequently formed the quantum dots<sup>S2</sup>. In sample B, a 2 nm CdTe quantum well (QW) layer was first deposited onto the ZnTe buffer. The deposition of amorphous Te was avoided by reducing the time for which the substrate was cooled under Te flux. In this way, QD formation was induced while preserving the quantum well (wetting layer), and the dot density was higher than in sample A. In both structures, quantum dots were capped by a 100 nm ZnTe layer.

The structures were examined using transmission electron microscopy (TEM). A very small amount of cadmium was found in sample A, complicating quantitative analysis. This agrees with observation of low QD density in PL experiments on sample A. In case of sample B, Supplemental Fig. 1(a) shows a representative TEM image taken under bright field conditions. A clear diffraction contrast is observed as darker areas. Supplemental Fig. 1(b) shows energy-dispersive x-ray (EDX) image of the same sample as in (a), which reveals that the darker areas originate from an increased cadmium content. An approximately horizontal ( $\sim 2^\circ$  tilt) cadmium-rich layer is observed in the EDX image and is attributed to the CdTe quantum well. The EDX image also reveals the inhomogeneity of Cd within the QW layer. Since the bright field image has better signal to noise ratio than EDX, we use the former to examine the scales of fluctuations of cadmium content. The arrows in Supplemental Fig. 1(a) mark the approximate boundary lines enclosing the two dark areas corresponding to increased Cd content. We attribute these cadmium-rich areas to QDs observed in PL experiments, and from the image we find that the dots have approximately cylindrical shape with a diameter of  $\sim 10$  nm and a height of  $\sim 2.5$  nm. Using the lattice constant of CdTe  $a_0 = 0.648$  nm, and taking into account that there are 8 atoms per cell, we estimate that a typical quantum dot contains  $\sim 5000$  atoms of all

isotopes (with and without nuclear magnetic moments).

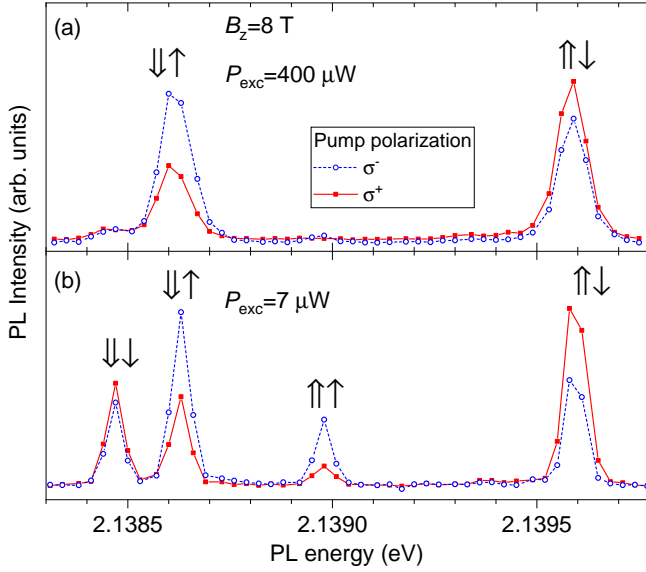


Supplemental Figure 1. (a) Representative transmission electron microscopy (TEM) image taken on sample B under bright field conditions. The arrows mark the approximate boundary lines of the two areas attributed to CdTe quantum dots. (b) Energy-dispersive x-ray (EDX) image of the same sample area as in (a) showing distribution of cadmium atoms.

### Supplemental Note 2. DERIVATION OF ELECTRON AND HOLE $g$ -FACTORS

Supplemental Fig. 2 shows photoluminescence spectra of a single quantum dot in sample A measured in high magnetic field  $B_z = 8$  T. The spectra were recorded under  $\sigma^-$  (dashed lines) and  $\sigma^+$  (solid lines) excitation at two different powers of  $P_{\text{exc}} = 400$   $\mu\text{W}$  (a) and  $P_{\text{exc}} = 7$   $\mu\text{W}$  (b). The high power spectrum consists of a Zeeman doublet corresponding to the bright exciton states  $\uparrow\downarrow$  and  $\downarrow\uparrow$ , where  $\uparrow$  ( $\downarrow$ ) denotes heavy hole states with momentum  $j_z = +3/2$  ( $-3/2$ ), while  $\uparrow$  ( $\downarrow$ ) denotes electron states with spin  $s_z = +1/2$  ( $-1/2$ ). At low power two additional lines appear – these correspond to recombination of the nominally dark states  $\uparrow\uparrow$  and  $\downarrow\downarrow$  made visible by mixing with the bright states in a low symmetry potential of the quantum dot<sup>S3,S4</sup>. From the low power spectrum we observe that each circularly polarized excitation enhances one bright and one dark transition. For example, the  $\sigma^-$  excitation enhances the low energy bright and the high energy dark transition, and since hole spin is usually lost during relaxation, we can deduce that these two states have the same electron spin projection. This observation allows the spectral lines to be assigned to the exciton states. There are two possible options: one is shown in Supplemental Fig. 2(b), and the other one has all electron and hole spin projections reversed. As we now show the correct assignment can be obtained from electron and hole  $g$ -factor calculations.

The energies of the bright excitons  $E_b$  and dark exci-



Supplemental Figure 2. Photoluminescence spectra of a quantum dot in sample A at  $B_z=8$  T measured under  $\sigma^-$  (dashed lines) and  $\sigma^+$  (solid lines) excitation at (a) high power  $P_{\text{exc}} = 400 \mu\text{W}$ , and (b) low power  $P_{\text{exc}} = 7 \mu\text{W}$ .

tons  $E_d$  can be written as follows<sup>S4-S6</sup>:

$$E_b = E_0 + \frac{\delta_0}{2} \pm \frac{1}{2} \sqrt{\delta_b^2 + \mu_B^2 (g_h - g_e)^2 B_z^2},$$

$$E_d = E_0 - \frac{\delta_0}{2} \pm \frac{1}{2} \mu_B (g_h + g_e) B_z, \quad (1)$$

where  $\mu_B$  is Bohr magneton,  $E_0$  – QD band-gap energy,  $g_e(g_h)$  – electron (hole)  $g$ -factor,  $\delta_0$  is the splitting between dark and bright exciton doublets,  $\delta_b$  is the bright doublet fine structure splitting, and we have neglected the overall diamagnetic shift and a small dark exciton fine structure splitting. For the dot shown in Supplemental Fig. 2, we find  $\delta_b \approx 60 \mu\text{eV}$  from PL spectra in low magnetic field. Using this value and the energies of the four exciton transitions, we calculated the  $g$ -factors  $g_e \approx \mp 0.49$  and  $g_h \approx \pm 1.59$ , where the two sign combinations correspond to the two possible assignments of the electron and hole spin states in the PL spectrum. The bulk electron  $g$ -factors are negative both in CdTe ( $g_e \approx -1.59$ , Ref.<sup>S7</sup>) and ZnTe ( $g_e \approx -0.6$ , Ref. <sup>S8</sup>), suggesting that it should be negative in CdTe/ZnTe quantum dots, as was observed previously<sup>S9</sup>. Thus we conclude that  $g_e \approx -0.49$  and  $g_h \approx +1.59$  and the correct assignment of the spin states is the one shown in Supplemental Fig. 2(b).

Measurements on several individual QDs in sample A have revealed very similar values of  $g_e$  and  $g_h$ . Dark exciton emission was not observed in sample B, but the Zeeman splitting of the bright states determined by  $g_h - g_e$  is found to be very similar to sample A, suggesting the individual  $g_e$  and  $g_h$  values are also similar. Recombination of a  $\uparrow\downarrow$  state results in emission of a circularly polarized photon with a +1 momentum – throughout this work we

label this polarization as  $\sigma^+$ . Conversely, excitation in  $\sigma^-$  polarization results in enhanced emission from the  $\downarrow\uparrow$  state.

### Supplemental Note 3. DERIVATION OF THE SIGN OF THE NUCLEAR SPIN POLARIZATION

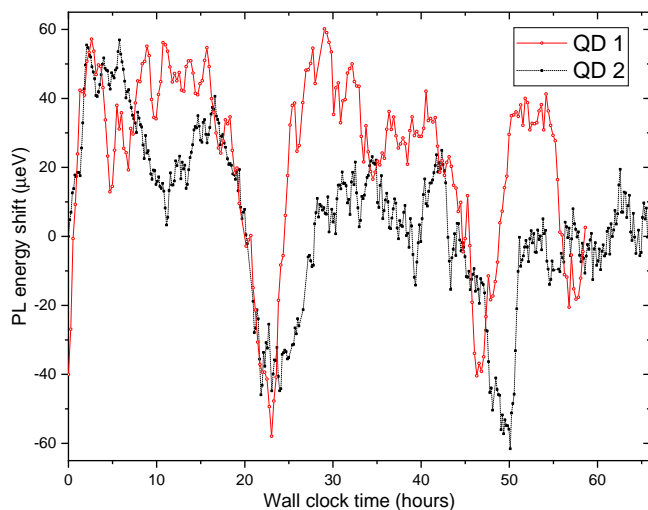
The Hamiltonian of the hyperfine interaction between the electron with spin  $\hat{s}$  and a nucleus with spin  $\hat{\mathbf{I}}$  is  $\hat{H}_{hf} = A(\hat{s} \cdot \hat{\mathbf{I}})$ . The hyperfine constant is  $A = (2\mu_0/3)\hbar\gamma_N g_e \mu_b |\psi(0)|^2$  (Ref.<sup>S10</sup>) where  $g_e \approx 2$  is the free electron  $g$ -factor,  $\mu_0$  is magnetic constant,  $\mu_b$  is Bohr magneton,  $\hbar$  is Planck constant, and  $|\psi(0)|^2$  is the electron wavefunction density at the site of a nucleus with gyromagnetic ratio  $\gamma_N$ . It can be seen that the sign of  $A$  is determined by the sign of  $\gamma_N$ . The underlying mechanism of dynamic nuclear polarization in quantum dots is the spin conserving electron-nuclear flip-flops made possible by the hyperfine interaction<sup>S11</sup>. If electrons with positive (negative)  $z$  spin projection are repeatedly injected into the dot via optical excitation with circularly polarized light, the resulting net nuclear spin polarization  $\langle I_z \rangle$  is also positive (negative). Generation of spin polarized electrons is evidenced for example in PL spectra of Fig. 1(c) and Supplemental Fig. 2 where  $\sigma^+$  ( $\sigma^-$ ) optical excitation preferentially enhances the population and PL intensity of a high- (low-) energy bright exciton Zeeman state. The spin-conserving nature of the flip-flop process implies that the signs of the non-equilibrium electron and nuclear spin polarizations are the same, so that the scalar product  $(\hat{s} \cdot \hat{\mathbf{I}})$  is always positive. Thus when nuclear polarization  $\langle I_z \rangle$  back-acts on the electron spin via hyperfine interaction, the sign of the energy shift (Overhauser shift) of the corresponding exciton state depends only on the sign of  $A$ . For example, in III-V semiconductors all nuclei have positive  $\gamma_N$  and  $A > 0$ . As a result the exciton state that is populated preferentially by the circularly polarized light shifts to higher energy – this statement is true both for the exciton with electron spin  $s_z = +1/2$  and the exciton with  $s_z = -1/2$  as observed e.g. in GaAs quantum dots<sup>S12</sup>. In the studied CdTe/ZnTe dots all of the Cd and Te isotopes (which are the most abundant) have  $\gamma_N < 0$  and hence  $A < 0$ . Thus the exciton state, whose PL intensity is enhanced under cw circularly polarized excitation is expected to shift to lower energy due to the resulting nuclear spin polarization.

In both structures studied here  $\sigma^+$  ( $\sigma^-$ ) excitation enhances PL intensity of the high (low) energy exciton state, as observed in Fig. 1(c) of the main text for a QD in sample A. The Overhauser shifts can be probed in pump-probe measurements as discussed in the main text. For sample B we find that nuclear spin polarization induced by  $\sigma^+$  ( $\sigma^-$ ) excitation decreases (increases) exciton Zeeman splitting  $E_Z$  measured in pump-probe, i.e. the exciton state whose population is enhanced by circularly polarized excitation shifts to lower energy. This

agrees with analysis above and confirms that nuclear spin polarization in sample B is produced by spin-conserving electron-nuclear flip-flops. By contrast, cw experiments on sample A show that Zeeman splitting under  $\sigma^+$  pumping can both increase and decrease depending on the individual quantum dot. This further confirms that the spectral shifts observed in sample A are not related to nuclear spin effects.

#### Supplemental Note 4. SPECTRAL WANDERING IN PHOTOLUMINESCENCE OF THE CdTe/ZnTe QUANTUM DOTS

Supplemental Fig. 3 shows variation of photoluminescence energies over the experiment duration (NMR spectra measurements). The results are shown for two different quantum dots (QD1 and QD2) from sample B, and it can be seen that spectral wandering is within  $\sim 100$   $\mu\text{eV}$  over the time scales of hours. Spectral wandering<sup>S13</sup> arises from the changes in the charge environment<sup>S14</sup> induced by continuous optical excitation, and reduces the accuracy with which the spectral splitting can be deduced from the photoluminescence signal. In the studied structures spectral wandering was found to differ significantly from dot to dot. Thus for the detailed studies of the nuclear spin phenomena, where small changes in spectral splitting need to be measured accurately, we have selected quantum dots with minimal wandering, such as those shown in Supplemental Fig. 3.



Supplemental Figure 3. Variation of the photoluminescence energy of the ground state neutral exciton as a function of the wall clock time under optical excitation. Data shown for two separate experiments on two different quantum dots.

#### Supplemental Note 5. DETAILS OF NMR TECHNIQUES

Optically detected nuclear magnetic resonance (NMR) spectra are measured using a pump-probe protocol consisting of the following steps: (i) nuclear spins are first polarized using circularly polarized light, (ii) a radio frequency (RF) pulse is applied without optical excitation to depolarize the nuclei selectively, (iii) nuclear spin polarization is finally detected by measuring QD PL under a short probe laser pulse. This cycle is typically repeated several hundred times for each radio frequency in order to accumulate probe PL signal sufficient for accurate derivation of the PL spectral splitting.

We use the “saturation NMR” measurement, where the frequency of a weak RF field is scanned to record the spectrum. The main difference from conventional saturation NMR is that a harmonic RF field of frequency  $f_{\text{RF}}$  is replaced by a RF field with a rectangular spectral band centered at  $f_{\text{RF}}$ . This spectral band is approximated by a “frequency comb” which is a sum of equally spaced harmonic modes. The mode spacing in our experiments is kept at  $f_{\text{ms}} = 125$  Hz. The total width of the band formed by the comb  $w_{\text{exc}}$  is chosen to be between few kHz and few hundred kHz depending on the measurement. This approach has been used previously for NMR spectroscopy of III-V semiconductor quantum dots<sup>S15</sup>. The advantage of the rectangular band RF is that  $w_{\text{exc}}$  can be varied to balance NMR signal amplitude and spectral resolution. For example, with a larger  $w_{\text{exc}}$  a larger fraction of nuclei is depolarized at each  $f_{\text{RF}}$ , resulting in a larger change in spectral splitting and hence improved NMR signal to noise ratio. At the same time, all NMR spectral features narrower than  $w_{\text{exc}}$  are averaged out, so that larger  $w_{\text{exc}}$  limits the resolution. The duration of the RF pulse  $T_{\text{RF}}$  in NMR spectral measurements is chosen based on an additional experiment with large  $w_{\text{exc}}$  covering the entire resonance and variable  $T_{\text{RF}}$ : the exponential depolarization time of the nuclear spins  $\tau$  is derived from such a calibration measurement and  $T_{\text{RF}}$  is set to  $\sim 5\tau$  for NMR spectroscopy.

Cadmium has two stable spin-1/2 isotopes:  $^{111}\text{Cd}$  with gyromagnetic ratio  $\gamma_{^{111}\text{Cd}}/(2\pi) \approx -9.06915$  MHz/T and  $^{113}\text{Cd}$  with  $\gamma_{^{113}\text{Cd}}/(2\pi) \approx -9.48709$  MHz/T (Ref. S16). Within the volume of a quantum dot the two types of Cd are distributed randomly so that on average, both isotopes experience the same statistical distributions of the chemical shifts and Knight fields. As a result, the NMR spectral lineshape of  $^{113}\text{Cd}$  is approximately the NMR spectrum of  $^{111}\text{Cd}$  but with all frequencies multiplied by  $\gamma_{^{113}\text{Cd}}/\gamma_{^{111}\text{Cd}}$ . Here we use this property to increase the magnitude of the NMR signal by measuring the response of  $^{111}\text{Cd}$  and  $^{113}\text{Cd}$  simultaneously. In Cd NMR experiments the spectrum of the RF excitation consists of two rectangular bands (frequency combs) of the same intensity centered at frequencies  $f_{\text{RF}}$  and  $(\gamma_{^{113}\text{Cd}}/\gamma_{^{111}\text{Cd}})f_{\text{RF}}$ . The value of  $f_{\text{RF}}$  is stepped in the experiment and is plotted on the horizontal axis of Fig. 4 of the main text. The

resulting Cd NMR spectra correspond to the  $^{111}\text{Cd}$  NMR lineshape which is amplified by adding a  $^{113}\text{Cd}$  lineshape with properly rescaled frequencies.

- 
- \* [gragunathan1@sheffield.ac.uk](mailto:gragunathan1@sheffield.ac.uk)  
 † [Jakub.Kobak@fuw.edu.pl](mailto:Jakub.Kobak@fuw.edu.pl)  
 ‡ [e.chekhovich@sheffield.ac.uk](mailto:e.chekhovich@sheffield.ac.uk)
- S1. F. Tinjod, B. Gilles, S. Moehl, K. Kheng, and H. Mariette, *Appl. Phys. Lett.* **82**, 4340 (2003).  
 S2. J. Kobak, J.-G. Rousset, R. Rudniewski, E. Janik, T. Slupinski, P. Kossacki, A. Golnik, and W. Pacuski, *J. Cryst. Growth* **378**, 274 (2013).  
 S3. T. Smoleński, T. Kazimierczuk, M. Goryca, T. Jakubczyk, L. Kłopotowski, L. Cywiński, P. Wojnar, A. Golnik, and P. Kossacki, *Phys. Rev. B* **86**, 241305 (2012).  
 S4. E. A. Chekhovich, A. B. Krysa, M. S. Skolnick, and A. I. Tartakovskii, *Phys. Rev. B* **83**, 125318 (2011).  
 S5. M. Bayer, G. Ortner, O. Stern, A. Kuther, A. A. Gorbunov, A. Forchel, P. Hawrylak, S. Fafard, K. Hinzer, T. L. Reinecke, S. N. Walck, J. P. Reithmaier, F. Klopff, and F. Schäfer, *Phys. Rev. B* **65**, 195315 (2002).  
 S6. M. Bayer, O. Stern, A. Kuther, and A. Forchel, *Phys. Rev. B* **61**, 7273 (2000).  
 S7. A. Nakamura, D. Paget, C. Hermann, C. Weisbuch, G. Lampel, and B. Cavenett, *Solid State Commun.* **30**, 411 (1979).  
 S8. G. Schmieder, W. Maier, L. Pu-Lin, and C. Klingshirn, *J. Lumin.* **28**, 357 (1983).  
 S9. Y. Léger, L. Besombes, L. Maingault, and H. Mariette, *Phys. Rev. B* **76**, 045331 (2007).  
 S10. C. P. Slichter, *Principles of Magnetic Resonance*, corrected third ed. (Springer, 1996).  
 S11. E. A. Chekhovich, A. Ulhaq, E. Zallo, F. Ding, O. G. Schmidt, and M. S. Skolnick, *Nature Materials* **16**, 982 (2017).  
 S12. E. A. Chekhovich, I. M. Griffiths, M. S. Skolnick, H. Huang, S. F. C. da Silva, X. Yuan, and A. Rastelli, *Phys. Rev. B* **97**, 235311 (2018).  
 S13. S. A. Blanton, M. A. Hines, and P. Guyot-Sionnest, *Appl. Phys. Lett.* **69**, 3905 (1996).  
 S14. J. Houel, A. V. Kuhlmann, L. Greuter, F. Xue, M. Poggio, B. D. Gerardot, P. A. Dalgarno, A. Badolato, P. M. Petroff, A. Ludwig, D. Reuter, A. D. Wieck, and R. J. Warburton, *Phys. Rev. Lett.* **108**, 107401 (2012).  
 S15. E. A. Chekhovich, K. V. Kavokin, J. Puebla, A. B. Krysa, M. Hopkinson, A. D. Andreev, A. M. Sanchez, R. Beanland, M. S. Skolnick, and A. I. Tartakovskii, *Nature Nanotechnology* **7**, 646 (2012).  
 S16. R. K. Harris, E. D. Becker, S. M. Cabral De Menezes, R. Goodfellow, and P. Granger, *Concepts in Magnetic Resonance* **14**, 326 (2002).